

The Portil∞: a deep learning-based open science tool for closed-loop brain stimulation

Nicolas Valençon, Yann Bouteiller, Hugo R. Jourde, Emily B.J. Coffey and Giovanni Beltrame

Abstract—Electroencephalography (EEG) is a method of measuring the brain’s electrical activity, using non-invasive scalp electrodes. In this article, we propose the Portil∞, a deep learning-based portable and low-cost device enabling the neuroscience community to capture EEG, process it in real time, detect patterns of interest, and respond with precisely-timed stimulation. The core of the Portil∞ is a System on Chip composed of an Analog to Digital Converter (ADC) and a Field-Programmable Gate Array (FPGA). After being converted to digital by the ADC, the EEG signal is processed in the FPGA. The FPGA contains an ad-hoc Artificial Neural Network (ANN) with convolutional and recurrent units, directly implemented in hardware. The output of the ANN is then used to trigger the user-defined feedback. We use the Portil∞ to develop a real-time sleep spindle stimulating application, as a case study. Sleep spindles are a specific type of transient oscillation (~ 2.5 s, 12-16 Hz) that are observed in EEG recordings, and are related to memory consolidation during sleep. We tested the Portil∞’s capacity to detect and stimulate sleep spindles in real time using an existing database of EEG sleep recordings. With 71% for both precision and recall as compared with expert labels, the system is able to stimulate spindles within ~ 300 ms of their onset, enabling experimental manipulation of nearly the entire spindle. The Portil∞ can be extended to detect and stimulate other neural events in EEG. It is fully available to the research community as an open science project¹.

I. INTRODUCTION

Electrical activity within the brain forms the basis of perception, thought and behaviour. This endogenous electrical activity tends to be oscillatory in nature, as reciprocal connections within and between brain regions form functional circuits for processing and communicating information, and it can be measured on the scalp using electroencephalography (EEG). Correlational studies have been performed for nearly a century that attempt to link specific patterns and frequency bands in EEG to cognitive functions or brain states. These studies are informative and increased our understanding of brain processes. However, they are unable to establish causal relationships. The ability to interact with brain oscillations in a precisely-timed fashion to enhance or inhibit endogenous processes - using sensory [1], [2], [3], [4], electrical [5] or magnetic [6] stimulation - allows for their functional roles to be determined [7], and potentially for restoration of processes deteriorated by aging or pathology [8]. While there is a great deal of interest in *closed-loop* stimulation [7], [9], researchers lack flexible, powerful tools that are easily accessible. Research efforts are also limited by the portability of systems, and by their complexity and expense. In the current work, we develop the *Portil∞*, a complete, portable system for

closed-loop stimulation. We demonstrate the Portil∞ on a case study of scientific relevance: the auditory stimulation of sleep spindles.

Using auditory stimulation, researchers have enhanced *slow oscillations* (SOs), which are high amplitude waves (0.5 - 1.5 Hz) known to be involved in memory consolidation [1]. Ngo *et al.* showed SOs enhancement caused an overnight improvement in memory performance, a result that has now been replicated (see [10], [11], [12] for reviews). Slow oscillations are thought to work in concert with other faster oscillations, called *sleep spindles*, to reactivate recently learned memories and transfer them to long-term memory [13], [14]. Sleep spindles are transient oscillations observed in both lighter and deeper non-rapid eye movement (NREM) sleep (*i.e.*, stages 2 and 3). Their role in memory consolidation is supported by increases in spindle density following learning (*e.g.*, [15]). Age-related changes in sleep spindles are correlated with differences in overnight performance gains (*e.g.*, [16], [17]; see [18] for a review of spindle mechanisms and functions).

Unfortunately, current systems that are capable of slow oscillation stimulation have more difficulty accurately and precisely detecting and stimulating sleep spindles in real time. Particular challenges of spindle stimulation are that each oscillatory cycle is only ~ 60 ms long and the entire spindle is between 0.5 and 2.5 s, leaving little time for traditional window-based frequency analysis; there is considerable variability between the frequency, amplitude, and duration of individuals’ spindles, particularly in older populations [19], [20]; and even for offline detection of spindles (which is an easier problem as the entire spindle is available and can be used in detection), agreement on spindle identification between experts and algorithms is limited ($\sim 70\%$) [21], [22].

If it were possible to influence spindles with sound, as it is to enhance slow oscillations, researchers could explore their functional role in healthy adults as well as characterize their involvement in cognitive aging, and even perhaps restore degraded function. Although auditory stimulation is attractive due to its non-invasiveness, it is only one of several possibilities: specific brain areas can be more directly and forcefully stimulated using transcranial electrical or magnetic stimulation, which could also be triggered by the same device. Furthermore, by designing the system flexibly such that it can be extended to detect and stimulate brain oscillations other than spindles, we can greatly expand its application, for example to theta-band oscillations that are associated with working memory capacity and task performance [23].

The goal of this work is to design and explore the properties of a deep learning-based, portable, battery-efficient and low-

¹<https://github.com/mistlab/portiloo>

cost device that will enable the neuroscience community to collect and process EEG data in real-time, detect patterns of interest for fundamental research questions, and respond at low latency with precisely-timed stimulation. We propose a neural network-based detection algorithm in FPGA and a parallelized design space exploration algorithm to optimize its parameters. We aim to accelerate fundamental research on closed-loop stimulation in neuroscience by creating a highly functional device and offering the code and plans to developers and scientists in the research community.

II. RELATED WORK

A. Devices for EEG acquisition and stimulation

Various portable devices have been developed to acquire and process EEG signals. In [24], the authors developed a low-cost device limited to acquisition. Other portable devices enable closed-loop stimulation [2], [3], [4], some also based on low-cost hardware [25], but work with simple heuristics and are generally not sufficiently powerful for deep learning applications. Closed-loop stimulation has been used in the context of preventing drowsiness [2], enhancing attention and engagement [4], preventing strokes [3] and studying memory consolidation [1], [25], [26], [27]. Depending on the application, real-time constraints can vary from hundreds of ms [28] to a few seconds [4]. The Portiloop is the first system to provide a portable, real-time and deep learning-based solution for all these applications.

B. Offline sleep spindle detection

Machine learning-based detection algorithms require large sets of accurately labeled data. The consistent detection and labeling of sleep spindles is a challenging task, due to variability in their appearance and strength. Traditionally, spindles are visually identified by experts. One commonly used dataset [29], [30] is the Montreal Archive of Sleep Studies (MASS) [31], in which the sleep spindle annotations were provided by two experts. Projects using MASS for training usually take spindles identified by either expert. However, the MASS annotations have a low inter-rater agreement, as quantified by the $f1\text{-score}^2$ of 0.54 [22]. The Massive Online Data Annotation (MODA) [22] project addressed this issue by having 5 experts (on average) annotate spindles and rate their confidence, in each EEG segment. The experts had an inter-rater $f1\text{-score}$ of 0.72 with respect to the final MODA labels. This score is considerably better than the MASS equivalent, and the number of experts, the scoring and the post-processing steps enable final labels of much higher precision.

Several offline sleep spindle detectors have been developed and tested on MODA [21], [32], [33], [34], [35], [36], [37]. However, these are generally heuristics that compute Fourier transforms or wavelet decomposition on large portions of the signal, including segments that would be in the future considering an online application, and thus cannot be implemented for real-time detection.

²The $f1\text{-score}$, widely used in statistics, is described in Equation 6.

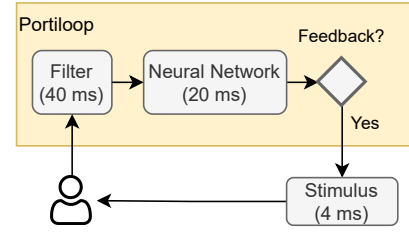


Fig. 1. Main functionalities. Timing is reported from our case study. The constant delay in stimulation output (4 ms for auditory stimuli) enables precise experimental control stimulation timing relative to neural oscillatory phase.

C. Online sleep spindle detection

Online detectors (*i.e.*, attempting detection during signal acquisition) face more challenging conditions than offline detectors, due to the unavailability of “future” data points. For example, the duration of the spindle is not yet known, and it is one of the identifying criteria commonly used by experts. Some existing heuristics filter the signal, compute power features and rely on thresholds to perform detection [25]. Yet, these approaches exhibit poor $f1\text{-scores}$. Deep learning can also be leveraged to perform online sleep spindle detection. This is done by first training an artificial neural network offline through supervised learning to detect sleep spindles, and then feeding the incoming signal to the trained detector. Several such models have been trained in previous work [29], [30], [38], [39]. However, these works do not consider hardware constraints that are central for our purpose: they use large models that are often unable to run in real time even on high-end GPUs, which makes them inapplicable on the Portiloop device. Moreover, they are usually trained and tested on MASS [31] with an ‘OR’ operation performed on its labels, and therefore limited performance [22]. In this work, we design a Pareto-optimal neural architecture that performs best on the MODA dataset [22] while satisfying our hardware and timing constraints. We validate our architecture against the state-of-the-art SpindleNet [29], initially used with the MASS dataset. When both architectures are trained and tested on MODA, ours outperforms the baseline, on top of running in real time with our hardware.

III. METHODS

A high-level description of the Portiloop system is provided in Figure 1. After being retrieved from the subject by electrodes and converted to numeric format by an Analog to Digital Converter (ADC), the EEG signal is processed through Finite Impulse Response (FIR) filters and fed to a trained Artificial Neural Network (ANN). The output of the ANN determines the nature of the feedback, *i.e.*, whether to stimulate the subject or not. These operations introduce their own constant delays in the closed-loop system (in Figure 1; note that the delays are measured on the sleep spindle detector that we derive in the second part of this article). Such delays are inherent to the order of the FIR filters, the architecture of the ANN and the nature of the stimulation. They have to be accounted for when building a Portiloop application, in order to satisfy the real-time constraints of the task.

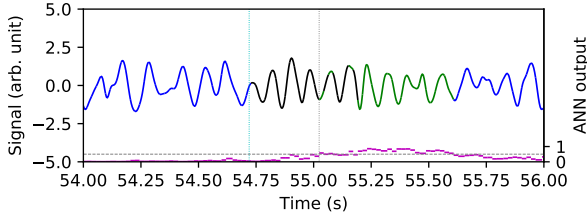


Fig. 2. Software accumulation effect of recurrent units. Dark blue signal: no phenomenon of interest. Black signal: phenomenon of interest not detected by the ANN. Green signal; phenomenon of interest correctly detected. Magenta: output of the ANN. Horizontal grey: detection threshold. The ANN introduces a software delay: the recurrent units of the ANN act as pseudo-accumulators, thus the detection happens with a variable delay.

A. Real-time constraints

To allow maximum flexibility in when the spindle can be stimulated, it must be accurately detected as early as possible following spindle onset. We identify two different sources of delay in the proposed system, *hardware* and *software* delays:

1) *Hardware delays*: By *hardware delays* we refer to the time it takes to retrieve the signal from the electrodes, convert it to digital, filter it, process it through the ANN, and send the resulting feedback stimulation to the subject.

Because we implement the Portiloop in Fast Programmable Gate Array (FPGA) logic, all these delays are constant. The hardware delays introduced by the electrodes, ADC and filtering are negligible in the Portiloop applications (*i.e.*, $\ll 1$ ms). The ANN delay depends on our implementation of the neural network architecture in FPGA. Since intra-layer operations can be parallelized in FPGA, it depends primarily on the depth of the ANN, *i.e.*, its number of layers. However, parallelization in FPGA has a cost in terms of resources, which are limited in the Portiloop. Thus, in practice, the width of reasonably large ANNs also has an impact on this delay. Finally, the stimulation delay depends on the nature of the stimulation. The Portiloop instantly sends a trigger from the ANN output, but this does not mean that the stimulus reaches the subject simultaneously, *e.g.*, 4 ms in the case of auditory stimulation.

2) *Software delays*: Although the hardware operations performed by FIR filters are near-instantaneous, this type of filtering introduces a constant software delay in the filtered signal. This delay is a trade-off related to the order of the FIR filter. The higher the order of a FIR filter, the more efficient it is at filtering out undesirable frequencies, but also the longer the software delay introduced in the signal by the filtering operation. More precisely, the delay d introduced by an FIR filter of order o on a signal sampled at frequency f is $d \propto \frac{o}{2f}$. These hardware and software delays sum to a constant total delay that is the minimum possible response time of the Portiloop system. Depending on the target timing constraints of the application, this leaves a certain margin for the actual detection of the phenomenon of interest in the filtered EEG signal. In practice, this detection may happen with its own variable software delay. An example of such delay is illustrated in Figure 2, where an ANN takes a variable amount of time before correctly detecting a transient pattern in an EEG signal.

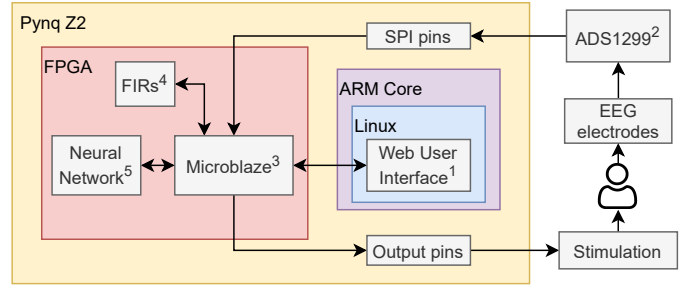


Fig. 3. Detailed architecture of the Portiloop device. (1) The user controls the device from a simple Web User Interface. (2) An EEG front-end device acquires biosignals from the electrodes. (3) The Microblaze soft processor centralizes all operations performed within the FPGA. (4) The Microblaze core sends the digital signal to be filtered through Finite Impulse Response filters. (5) The Microblaze core sends the digital filtered signal to an artificial neural network. The neural network returns the likelihood of the input signal being the desired pattern in order to decide whether a stimulus should be sent.

B. Architecture of the proposed system

The detailed architecture of the Portiloop device is presented in Figure 3. The system is implemented on a Pynq Z2 [40] board. This board provides an integrated FPGA, which we use along the Vivado suite (v2019.1) to convert our software logic into hardware circuitry operating in real time.

1) *Data acquisition*: The analog signal captured by the electrodes is processed by a low-noise ADC front-end for EEG/ECG developed by Texas Instrument (ADS1299 [41]). This component can retrieve signal from 8 electrodes simultaneously, plus reference and bias electrodes. The ADC outputs a digital signal, data point per data point. Each data point is sent directly to the Pynq Z2 board at up to 16 kHz through Serial Peripheral Interface (SPI) communication.

2) *Data preprocessing*:

a) *Microblaze*: The Microblaze is a soft processor that is readily implemented by Xilinx on the FPGA. It acts as a central scheduler for all operations happening within the FPGA. We use the Microblaze to read data points from the SPI pins in real time and log them for possible post-analysis. We send either each or a relevant fraction of these data points to the FIR filters in real time by Direct Memory Access (DMA).

b) *FIR filters*: We use FIR filters to preprocess the digital signal by filtering out undesired frequencies. These filters are readily available as Intellectual Property (IP) cores provided by Xilinx. We retrieve each unprocessed data point, filter it, and send the filtered data point back to the Microblaze through DMA. It is possible to implement as many FIR filters as needed, in the limit of the available space on the FPGA.

c) *Additional preprocessing*: We can further preprocess the filtered signal directly within the Microblaze for simple operations. In particular, we standardize the signal on the fly through exponential moving average. In other words, we transform the filtered signal $s(t)$ to $s'(t)$ according to:

$$s'(t) = \frac{s(t) - \hat{\mu}(t)}{\hat{\sigma}(t)} \quad (1)$$

where $\hat{\mu}$ and $\hat{\sigma}$ are estimates of the mean and standard deviation of the filtered signal, computed as follows:

$$\delta(t) = s(t) - \hat{\mu}(t-1) \quad (2)$$

$$\hat{\mu}(t) = \hat{\mu}(t-1) + \alpha_\mu \delta(t) \quad (3)$$

$$\hat{\sigma}^2(t) = (1 - \alpha_\sigma)(\hat{\sigma}^2(t-1) + \alpha_\sigma \delta^2(t)) \quad (4)$$

$$\hat{\sigma}(t) = \sqrt{\hat{\sigma}^2(t)} \quad (5)$$

α_μ and α_σ being hyperparameters in $[0, 1]$. This custom real-time standardization makes the signal comparable from one subject to another, enabling generalizable learning.

3) *Neural Network*: Any real-time decision-making algorithm can be implemented on the Portiloop as long as it is written in FPGA-ready code. We focus on ANN models. The Portiloop being a portable, lightweight and battery-efficient system, it does not include any heavy computing units such as high-end GPUs. Instead, the ANN is synthesized as hardware circuitry in an FPGA, which provides only a limited amount of configurable circuitry. Thus, only small ANN models are allowed. We provide High-Level-Synthesis (HLS) C++ implementation of the following building blocks, based on [42]:

- 1D convolutional layers, used to learn and extract relevant patterns (*e.g.*, frequencies) in the signal.
- Layers of Gated Recurrent Units (GRUs), used to learn a memory representation, so as to keep track of the past. GRUs are usually on par with their famous Long-Short Term Memory (LSTM) cousin in terms of performance [43], [44], but they use roughly 30% less hardware resource and thus are more interesting in the context of FPGAs, where resources are limited.
- Fully connected layers, used to further increase the representational capacity of the model.
- Rectified Linear Unit (ReLU) non-linearities, which are simple $\max(x, 0)$ operations with minimal footprint.

We train an ANN offline using PyTorch³, and once trained, we extract its weights from PyTorch and use our C++ library in the Vivado suite to convert the model (architecture and weights) into the FPGA. When a data point is fully preprocessed through the steps described in Section III-B2, the Microblaze sends a buffer of the last preprocessed data points by DMA to the ANN. In other words, we feed a sliding window of preprocessed signal as input to the model.

Inference is performed by the neural network in parallel to the acquisition and preprocessing of the next data point by the Microblaze. Once inference is done, the result is sent back to the Microblaze through DMA. Depending on this result, the Microblaze writes a code (*e.g.*, a trigger signal) on the output pins of the Portiloop device. Any stimulation device can be used with an appropriate adapter for the trigger signal.

C. Type of ANN

The Portiloop system is designed to process EEG signals in real time. This type of input involves time-series of data containing oscillatory and transitory elements. In the realm

of deep learning, a natural way of processing such data is to use either 1D convolutions, recurrent units, or a combination of both. The type of ANN architecture that we recommend is inspired by the SpindleNet [29] architecture. In essence, a sliding window over a few last data points is fed to a Convolutional Neural Network (CNN) whose purpose is to extract relevant features (*e.g.*, frequencies) in this signal fragment. Then, these extracted features are fed to a Recurrent Neural Network (RNN) whose purpose is to keep track of the features extracted in past forward passes. Note that another family of architectures, called Transformers [45], is known for exhibiting good results task-wise with this type of data. However, Transformers are memory-less and not suitable for lightweight real-time applications, because they need to process the whole signal at each forward pass. Conversely, RNNs are able to process one single data point at each forward pass and keep track of the past in memory, which makes them more relevant in Portiloop applications.

D. Pareto-optimal architecture search

The FPGA used in the Portiloop has a limited amount of available circuitry, so as to ensure its portability and low price. Thus, typically large ANN architectures such as SpindleNet [29] are orders of magnitude too large to be implemented in our device. Fortunately, as we illustrate in Section IV, those models are often much too large for their actual purpose. When developing a novel Portiloop application, one needs to devise a neural network that is both high-performance and lightweight, by selecting the right set of hyperparameters H in the space of all possible hyperparameter sets \mathcal{H} . Such hyperparameters include the size of the sliding window, the number of layers in each part of the ANN, the width of each layer, the time dilation (see Section III-E), the type of optimizer, the hyperparameters of the optimizer itself, etc. \mathcal{H} can be very large, and finding a set of hyperparameters that yields a high-performance model within given hardware constraints is far from trivial. We introduce ‘‘Parallel Model-Based Optimization’’ (PMBO), a network-based algorithm that automates this process in a parallel fashion. Released as open-source along with our code, PMBO is essentially a parallelized and evolved version of ‘‘Probabilistic SMBO’’ [46]. PMBO is a guided-search approach that finds a suitable set of hyperparameters rapidly. For this matter, it uses one machine (or process) to train a *meta network* whose role is to predict non-trivially available costs for any given set of hyperparameters. Furthermore, PMBO uses any available machines (or processes) in parallel to train ANNs from sets of hyperparameters selected based on the cost estimated by the meta model.

1) *Software and hardware costs*: The purpose of PMBO is to find Pareto-optimal sets of hyperparameters that minimize both a *software cost* and a *hardware cost*. Hyperparameter selection is a bi-objective problem in our setting:

- On the one hand, we want an ANN that performs well at detecting the desired patterns. We measure this performance in terms of the f1-score of our model. The f1-score depends both on the precision (how sure we are that positive outputs

³<https://pytorch.org/>

are true positives) and on the recall (how sure we are that we capture all true positives) of the model. It is defined as:

$$f1 = \frac{2 * \text{recall} * \text{precision}}{\text{recall} + \text{precision}} \quad (6)$$

where

$$\text{precision} = \frac{\text{true positives}}{\text{true positives} + \text{false positives}} \quad (7)$$

and

$$\text{recall} = \frac{\text{true positives}}{\text{true positives} + \text{false negatives}} \quad (8)$$

The f1-score is in $[0, 1]$, with 1 being a perfect classifier. We cast this into a minimization problem by defining our *software cost* as $L_s = 1 - f1$.

• On the other hand, we want our ANN to be as lightweight as possible, so it fits in the FPGA and executes as fast as possible. A precise measurement of the execution duration and amount of circuitry needed on the board is difficult. In fact, we do not have access to these results until the model is actually synthesized on the board, which is a long process. Thus, we use the number of trainable weights in the ANN as a proxy for these concerns, and call this number our *hardware cost* L_h . This cost is computed directly in PyTorch. Note that our choice of costs is arbitrary and other custom costs can be used instead.

2) *Pareto efficiency*: Let us consider a meta dataset \mathcal{E} of previously completed experiments (*i.e.*, tuples $E = (H, L_s, L_h)$) of hyperparameter sets with their real costs). Let us also consider the following Pareto-domination relation:

Definition 1. Let $E = (H, L_s, L_h)$ and $E' = (H', L'_s, L'_h)$ be two experiments in \mathcal{E} . We say that E Pareto-dominates E' and we denote $E < E'$ when $L_s < L'_s \wedge L_h < L'_h$. (NB: in the context of this minimization problem, dominating means having the smallest costs, hence the notation)

For a given experiment E and meta dataset \mathcal{E} , we denote $D_{\mathcal{E}}(E)$ as the number of experiments in \mathcal{E} that are Pareto-dominated by E , and $d_{\mathcal{E}}(E)$ as the number of experiments in \mathcal{E} that Pareto-dominate E . In other words:

$$D_{\mathcal{E}}(E) = |\{E^i \in \mathcal{E}, E^i > E\}| \quad (9)$$

$$d_{\mathcal{E}}(E) = |\{E^i \in \mathcal{E}, E^i < E\}| \quad (10)$$

For a given set of hyperparameters $H \in \mathcal{H}$, we further define an estimate of the corresponding completed experiment E as $\hat{E} = (H, \hat{L}_s, \hat{L}_h)$, where \hat{L}_s and \hat{L}_h are estimates of the real costs, computed by the meta network. Note that in our setting, $\hat{L}_h = L_h$ is available and thus only \hat{L}_s is estimated by the meta network. We propose the heuristic Pareto efficiency $\eta(\hat{E})$:

$$\eta(\hat{E}) = a_{\mathcal{E}}(\hat{E}) + b_{\mathcal{E}}(\hat{E}) + s_{\mathcal{E}}(\hat{E}) - h_{\mathcal{E}}(\hat{E}) \quad (11)$$

where $a_{\mathcal{E}}(\hat{E})$ promotes hyperparameter sets whose predicted costs are not dominated by many experiments in \mathcal{E} :

$$a_{\mathcal{E}}(\hat{E}) = 1 - \frac{d_{\mathcal{E}}(\hat{E})}{|\mathcal{E}|} \quad (12)$$

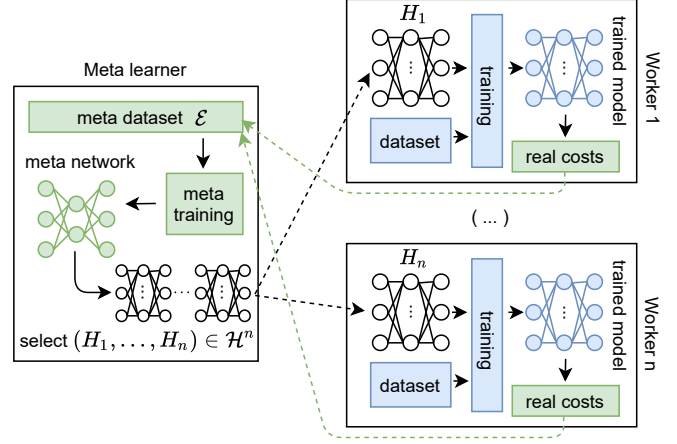


Fig. 4. PMBO. The algorithm is based on a single producer and multiple consumers architecture. The meta learner is in charge of producing relevant hyperparameter sets in a guided fashion. Then, it sends them to idle workers, and keeps producing new sets as long as idle workers remain. Each worker that has received a new set starts training the corresponding ANN. Once this training ends, the real costs of the hyperparameter set can be computed and are sent back to the meta learner.

$b_{\mathcal{E}}(\hat{E})$ promotes hyperparameter sets whose predicted costs dominate many experiments in \mathcal{E} :

$$b_{\mathcal{E}}(\hat{E}) = \frac{D_{\mathcal{E}}(\hat{E})}{|\mathcal{E}|} \quad (13)$$

$s_{\mathcal{E}}(\hat{E})$ promotes hyperparameter sets whose predicted software costs are better than the best software cost amongst all completed experiments in \mathcal{E} :

$$s_{\mathcal{E}}(\hat{E}) = \frac{\min(\{L_s, (H, L_s, L_h) \in \mathcal{E}\})}{\hat{L}_s} \quad (14)$$

and $h_{\mathcal{E}}(\hat{E})$ penalizes hyperparameter sets that have a high density with respect to experiments present in \mathcal{E} in terms of their hardware cost. More precisely, we define a range of hardware costs we are interested in, and we split this range into a number of bins. We then compute the binned density of experiments in \mathcal{E} over this range, and multiply this density by the range's width. The penalty $h_{\mathcal{E}}(\hat{E})$ is the height of the resulting bin where \hat{L}_h stands. Multiplying the density by the range's width enforces $h_{\mathcal{E}}(\hat{E}) > 1$ in regions of high density and $h_{\mathcal{E}}(\hat{E}) < 1$ in regions of low density.

3) *Parallel Model-Based Optimization*: Figure 4 explains the PMBO algorithm. A central meta learner is communicating with n peripheral workers to find a hyperparameter set $H^* \in \mathcal{H}$ that is Pareto-optimal for both the software and hardware costs (*i.e.*, non-Pareto-dominated by any other set). For this matter, the algorithm uses a meta dataset \mathcal{E} of tuples $E^i = (H^i, L_s^i, L_h^i)$ to train a meta network that maps any hyperparameter set $H \in \mathcal{H}$ to its corresponding (estimated) costs \hat{L}_s and \hat{L}_h ⁴. Once the meta network is trained, it is used to guide the sampling process. More exactly, we sample

⁴ \hat{L}_h is an output of the meta network in the general case. However, with our choice of hardware cost it is not, since the ground truth L_h is available.

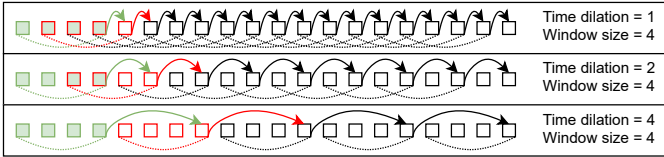


Fig. 5. Time dilation. In this example, a sliding window of the 4 last samples (underlined with a dotted curve) is used as input to the model. The time dilation is the number of samples between two forward passes in the ANN. When it is small (top), two consecutive windows overlap for the most part (see *e.g.*, green and red windows). This implies that the recurrent hidden state which persists from one forward pass to the next (arrows) contains a lot of redundancy with the next input. When the time dilation is big (bottom), this issue is corrected, and back-propagation will reach much further back in time for the same number of forward passes. NB: forward passes happen only at the end of arrows in this diagram, the ANN is idle during other time-steps.

m hyperparameter sets in \mathcal{H} from a multivariate Gaussian distribution around the hyperparameter set corresponding to the last results received from the workers by the meta learner. Sets that don't satisfy user-defined constraints (*e.g.*, that have already been tested, or, when L_h is available, that fall outside the range we are interested in) are discarded and resampled. We then select the best set in terms of Pareto efficiency, estimated thanks to the trained meta network. This selected set is appended to a bounded buffer, waiting to be consumed by an idle worker. The sampling process is repeated until the bounded buffer is full. When a worker is idle, it fetches an ANN architecture and training instructions from the bounded buffer. The worker yields a measurement of the real hardware and software costs for the current hyperparameter set, which are sent back to the meta learner and appended to the meta dataset. The meta learner then uses the updated meta dataset to train a new meta network, and so on.

E. Virtual ANN parallelization with time dilation

Time dilation [47] is a technique that enables recurrent units such as GRUs to look further back in time before gradients vanish, at no computational cost. We propose a version of this technique that allows us to virtually parallelize a single physical ANN into several decoupled virtual models. Our approach enables shallow recurrent neural networks to look further back in time by skipping the redundant information that is inherent to the use of a sliding window as input, while still acting as fast as possible. Figure 5 shows how time dilation can be used to look further back in time and avoid redundancy.

Although time dilation enables reaching further back in time at no extra computational cost, this comes with a cost in terms of delays. Since our technique causes samples⁵ to be skipped between forward passes in the ANN, a detection delay that can be as long as the time dilation is introduced. We correct this issue by implementing a trick that we call *virtual parallelization*. We create a First In First Out (FIFO) list as big as the time dilation, and fill this list with independent hidden states. At each time-step, we pop a hidden state from this list,

⁵Here, by *sample* we refer to all data points acquired while a forward pass is executed in the ANN. For the sake of simplicity, our figures assume that there is only one data point per sample.

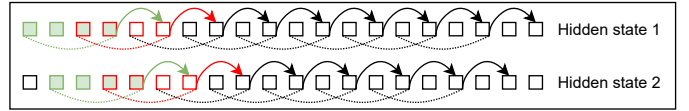


Fig. 6. Virtual parallelization. In this example, the time dilation is 2. Thus, we keep track of 2 independent hidden states and feed these alternately to the recurrent units of the ANN. This is equivalent to having two decoupled models that are used alternately for inference.

feed it to the recurrent units of our ANN, perform a forward pass, and append the resulting hidden state to the list. Doing this without skipping samples is equivalent to having several decoupled models running in parallel as illustrated in Figure 6, although one single ANN is physically used. This trick allows us to keep acting as fast as possible since it removes the need for skipping samples, while still reaching far back in time at no extra computational cost.

F. Case study: sleep spindle auditory stimulation

We now demonstrate the Portiloop implementation of stimulating the brain with sound during sleep spindles. The long-term goal of this application is to further clarify the role of sleep spindles in learning and memory, and to explore therapeutic interventions for memory decline. Stimulating sleep spindles is more challenging than low frequency neural activity like slow oscillations, due to their high frequency (~ 12 to 16 Hz), rapid evolution (< 2.5 s), and therefore tight timing constraints. We propose the first portable device able to stimulate sleep spindles in real time with high detection performance. Because maximum experimental flexibility is attained by being able to stimulate at anytime during the course of the spindle including with phase precision, we conduct a thorough time analysis of the proposed system, with possible trade-offs to maximize specific performance.

1) *Neural architecture*: To the best of our knowledge, the state-of-the-art in previous work regarding online sleep spindles detection was the SpindleNet [29] model. This architecture is however much too large to be implemented on the Portiloop system. Moreover, it is trained and evaluated on the MASS labels, which has been annotated by experts whose spindle evaluation varies considerably, and it is closed-source. Nevertheless, we draw inspiration from their work as a starting point for our ANN architecture design. In particular, we train models based on the same idea of using CNNs followed by RNNs, and we evaluate the relevance of the three different inputs used by SpindleNet (namely, the raw signal, the signal envelope and the power features) in our setting. We use PMBO along with the MODA dataset to derive a much smaller architecture, and provide a quantitative comparison with the SpindleNet architecture on MODA. Since we do not have access to the SpindleNet model, we rebuild the architecture described in [29] and train it on the MODA dataset with the same pipeline that we use to train our models.

2) *Dataset and training*: We use the MODA dataset, with ethics approval, for training our ANN, since its labels are considerably more reliable than *e.g.*, performing an 'OR'

operation on the MASS labels [22]. This dataset is divided in two subsets. The first one, called *phase 1*, consists of 100 younger subjects, whereas the second one, *phase 2*, consists of 80 older subjects. The MODA dataset provides two types of annotations (labels) on the signal: the first is the mean score given by the group of experts for each data point; the second is a binary classification of each data point as a spindle or non-spindle, defined by a threshold on the aforementioned scores (0.2 for phase 1 and 0.35 for phase 2). Further post-processing steps were applied to obtain these binary labels: spindles that were too short (< 0.3 s) and too close (< 0.1 s) to each other were merged, then spindles that were too short (< 0.3 s) or too long (> 2.5 s) were relabeled as negative. Given this dataset, two types of ANNs are possible: classifiers and regressors. These two types of ANNs differ only by the labels and losses used to train them. Classifiers are trained on the binary labels, by optimizing the binary cross entropy loss. They directly predict whether the current signal is a spindle or not, according to the very specific definition given by these binary labels (*i.e.*, taking into account the thresholds and post-processing applied by MODA). Regressors are trained on the score labels, by optimizing the mean square error loss. They predict the score given by the experts (before the aforementioned post-processing steps), which allows the user to select their own threshold for detection. Note that, in practice, classifiers also enable the user to select their own threshold, although in a less interpretable way. We experiment with both types of models. Finally, note that MODA is a highly unbalanced dataset as only about 5 % of the signal is labeled as sleep spindles. During the course of this work, we tried different ways of balancing training for classifiers and regressors. Interestingly, we found that classifiers highly benefit from oversampling (*i.e.*, sampling 50 % of spindles and 50 % of non-spindles from the dataset during training) whereas all the balancing techniques we tried for regression (including oversampling, Label Distribution Smoothing [48] and a custom version of the latter) actually hinder the training.

3) *Signal processing pipeline*: Because we use the SpindleNet architecture as a baseline to evaluate our approach, we need to compute all three inputs used by this model *i.e.*, a clean signal, an envelope of the signal, and a “power feature ratio” [29]. The latter compares frequencies between 2 Hz and 8 Hz with frequencies between 9 Hz and 16 Hz from the Fourier transform over the last 500 ms of signal. Computing this ratio is resource-intensive in the context of the Portilooop system, plus we found that this did not help our models. Therefore we compute this ratio offline for the sole purpose of comparison with the SpindleNet architecture; it is not used in our model. We set the ADC frequency to 500 Hz, which allows the Microblaze soft processor to log the raw signal at a finer-grained resolution than what we actually use for detection. The raw signal is then downsampled to 250 Hz. Figure 7 depicts the FPGA pipeline that computes cleaned signal and envelope.

Since FIR filters introduce software delays, we designed both branches of the pipeline so that they introduce identical software delays to their respective outputs (*i.e.*, 40 ms at 250 Hz sampling rate), see Figure 7. We used the same frequency band to prepare our ‘cleaned signal’ in the first

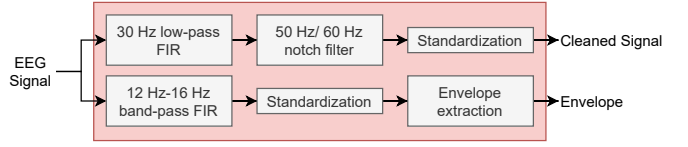


Fig. 7. Signal processing pipeline extracting relevant inputs for the ANN. Power features are computed offline only for the SpindleNet architecture and are not represented in this diagram.

step of the pipeline as is used in standard sleep scoring (*i.e.*, 0.5 Hz to 30 Hz) [49].

An FIR filter of order 10 works reasonably well to remove frequencies above 30 Hz, but we observed persistent power line noise. To address this issue, we apply a notch filter whose frequency depends on the geographical area (50 Hz in Europe, 60 Hz in North America). For removing low frequencies, we rely on the online standardization process described in Section III-B2c. We use a coefficient $\alpha_\mu = 0.1$ for our running average, which can be shown to attenuate frequencies under 4 Hz. We use a smaller coefficient $\alpha_\sigma = 0.001$ for our running variance, meaning that our estimate of the standard deviation takes a larger portion of the signal into account. We empirically found this choice of α_μ and α_σ to reveal EEG features of interest and yield sensible standardization, by visual inspection. We apply a similar procedure in the second branch to extract the envelope. First, the signal is filtered with a FIR band-pass between 12 Hz and 16 Hz. Then, it is standardized like in the first branch, except that we use $\alpha_\mu = \alpha_\sigma = 0.001$. We then square the signal and smooth the result by computing its moving average according to Equation 3, this time with $\alpha_\mu = 0.01$. This method is much simpler and faster than computing *e.g.*, an Hilbert envelope. We evaluate different types of ANN architectures, using either both or only one of these preprocessed signals as input.

4) *Stimulation*: The output of the ANN tells whether the model considers the current signal being a sleep spindle or not. Some further processing is necessary to ensure that we only send one stimulation per spindle. As seen in Figure 2, the detection can be noisy around the beginning or the end of a spindle, especially since we use decoupled virtual parallel networks (see Section III-E). A stimulation is sent upon initial spindle detection. To avoid multiple stimulations of the same spindle the subsequent stimulation may only occur once the current stimulus ended and at least 400 ms following the ending of the spindle. If a spindle is detected again within this duration the timer is reset, since we consider it as being part of the previous spindle.

IV. EXPERIMENTS

We devise a Pareto-optimal neural architecture using the PMBO algorithm. We conduct a thorough quantitative and qualitative study of the resulting system, not only in terms of ethereal detection scores as generally seen in previous work, but also in terms of real-time stimulation performance. Note that all our experiments are based on the MODA dataset rather than actual nights spent wearing the Portilooop device, as we

do not have ground truth labels for such data. Using the final device would require reproducing the experimental setting of MASS/MODA, which we leave to experts for future work.

A. Online detection

All results regarding online detection performance are summarized in Table I. This table shows the f1, precision and recall metrics that statistically describe how efficient different models are at detecting sleep spindles (on average over all data points). These metrics are provided separately for phase 1, which groups younger subjects, for phase 2, which groups older subjects, and for the whole cohort.

1) *Experts and offline detectors*: As previously highlighted, sleep spindle detection is a difficult task and experts themselves often do not agree when annotating these offline. This disagreement is quantified by MODA [22] and represented in Table I, row (1) for reference. The experts annotating the MODA dataset had an average performance of 0.72 on the whole cohort in term of the f1-score of their individual annotations w.r.t. the final labels. They are compared to other *offline detection*, *i.e.*, when a virtually infinite computational budget and the whole signal is available, including future data points, presented under “offline detection” in Table I (taken from [22]). We instead perform *online detection*, which has additional challenges: (a) computation happens in real time; (b) the future signal is not available.

2) *ANN training and evaluation*: The MODA dataset is relatively small (~ 24 h of annotated data) and heterogeneous. This adds some difficulty for training and properly assessing the performance of our models, because we choose to use only 10% of subjects as our validation set (for model selection), and another 10% of subjects as our test set (for final model evaluation). Since the overall results are dependent on the assignment of subjects to the three sets, we evaluate our models through the following procedure:

- we shuffle all subjects 10 times and compute a different training/validation/test split of the dataset each time;
- for each split, we use the training set to train 3 models, the validation set being used to estimate their f1-score. We select the best of these 3 models by its best f1-score on the validation set. We then report the performance of this model in terms of its f1-score on the test set;
- the above being repeated 10 times, we report the average test f1-score in Table I, the corresponding standard deviation being indicated in parenthesis.

3) *SpindleNet baseline*: The SpindleNet [29] architecture is far too large to be implemented on the Portiloop, and it cannot run in real time unless using a high-end GPU/TPU. Nevertheless, to the best of our knowledge, it is the state-of-the-art among previous work for the online detection of sleep spindles. Therefore, we use this architecture as a baseline for evaluating the performance of our own models, discovered via PMBO. Since SpindleNet is closed-source and trained on the MASS dataset, we retrain its architecture from scratch with the same pipeline as used to train our other classifiers. In particular, we balance training through oversampling (as opposed to the data augmentation technique used by the

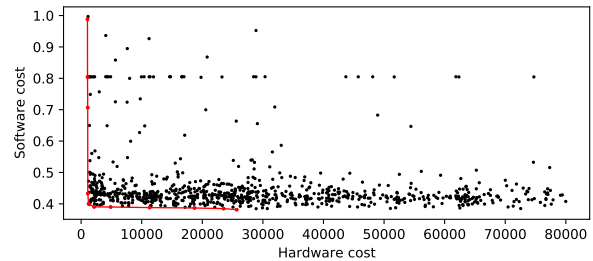


Fig. 8. Single-input architecture search with PMBO. The hardware cost is the number of trainable parameters in the neural architecture, and the software cost is $1 - \text{f1-score}$ of the fully-trained model. Black: non-Pareto-optimal models tested by the algorithm. Red dots: Pareto-optimal models found by the algorithm. Red line: Pareto front.

authors of the original paper), and more importantly we train and evaluate SpindleNet on the MODA dataset. The results of this experiment are presented in Table I, row (2).

4) *2-input model*: We first derive a lightweight ANN architecture by drawing inspiration from SpindleNet. More precisely, we use PMBO to find a Pareto-optimal architecture that uses both the cleaned signal and the envelope as inputs. The resulting architecture is presented in Appendix G⁶. Despite being small compared to the architectures commonly encountered in the literature, this architecture is still far too large to be synthesized in a fully-parallel fashion. Instead, the HLS compiler partially sequences operations in the FPGA. We measure a total duration of 40 ms for each forward pass in this model on the Portiloop. The detection performance of this model, reported in Table I, row (3), outperforms the baseline. This is not particularly surprising, as the baseline was originally designed using MASS rather than MODA.

5) *Envelope ablation*: The idea of using the envelope along the raw signal as input to the ANN is drawn from the baseline. Since the envelope is computed from the raw signal, it should not contain any additional information that cannot be extracted by an ANN in theory; we suspect it can be removed. To evaluate the relevance of this particular input, we perform the following ablation: to keep the same architecture (and thus the same model capacity), we replace one of the two inputs by a copy of the other. In Table I, row (4) both inputs are the envelope, while in row (5) both inputs are the cleaned signal. We find that the envelope input can be removed: the model in which we replace the envelope with a copy of the cleaned signal (5) has the same performance as the original model (3), and performs marginally better on phase 2.

6) *Single-input model*: Since we deemed the use of the envelope input ineffective in the ablation study, we use PMBO one more time to devise our final Pareto-optimal ANN architecture, now with only the cleaned signal as input. For this matter, we run PMBO on 20 Tesla V100 GPU workers over a period of 24h. The detailed hyperparameters used in this experiment are provided in Appendix C, and the results are visualized in Figure 8. PMBO brought the architecture search towards high-performance lightweight models. We select the best such model in terms of software cost *i.e.*, the model

⁶Appendices are available online at <https://mistlab.ca/papers/Portiloop/>

Table I. Quantitative results. The nomenclature is “mean (std)” and the superscripts are for referencing rows in the text.

	(a) Phase 1 (younger)			(b) Phase 2 (older)			(c) Whole Cohort		
	Recall	Precision	f1	Recall	Precision	f1	Recall	Precision	f1
<i>IExp</i> ¹	0.76 (0.16)	0.81 (0.17)	0.76 (0.1)	0.66 (0.19)	0.74 (0.17)	0.65 (0.12)	0.72 (0.18)	0.78 (0.17)	0.72 (0.12)
	Offline Detection								
<i>Ferrarelli</i> [32]	0.19	0.83	0.31	0.16	0.87	0.27	0.18	0.85	0.29
<i>Möller</i> [33]	0.83	0.47	0.6	0.78	0.44	0.56	0.81	0.46	0.58
<i>Martin</i> [34]	0.61	0.64	0.62	0.58	0.56	0.57	0.6	0.6	0.6
<i>Wamsley</i> [35]	0.57	0.69	0.63	0.56	0.62	0.59	0.57	0.66	0.61
<i>Lacourse</i> [21]	0.75	0.73	0.74	0.7	0.69	0.7	0.73	0.71	0.72
<i>Ray</i> [36]	0.73	0.47	0.57	0.75	0.32	0.45	0.74	0.4	0.51
<i>Parekh</i> [37]	0.85	0.61	0.71	0.74	0.68	0.71	0.8	0.65	0.71
	Online Detection								
<i>Based on SpindleNet</i> [29] ²	0.92 (0.04)	0.24 (0.07)	0.38 (0.07)	0.85 (0.06)	0.19 (0.08)	0.3 (0.1)	0.89 (0.05)	0.22 (0.07)	0.35 (0.08)
2-input ³	0.68 (0.04)	0.6 (0.06)	0.64 (0.03)	0.52 (0.09)	0.58 (0.04)	0.54 (0.05)	0.62 (0.06)	0.6 (0.05)	0.61 (0.03)
2-input ablation 1 ⁴	0.7 (0.09)	0.47 (0.08)	0.55 (0.04)	0.56 (0.11)	0.43 (0.09)	0.47 (0.04)	0.65 (0.1)	0.46 (0.08)	0.52 (0.04)
2-input ablation 2 ⁵	0.72 (0.03)	0.57 (0.06)	0.64 (0.03)	0.57 (0.08)	0.53 (0.04)	0.55 (0.04)	0.67 (0.04)	0.56 (0.05)	0.61 (0.03)
1-input ⁶	0.7 (0.04)	0.59 (0.05)	0.64 (0.03)	0.54 (0.09)	0.58 (0.05)	0.55 (0.05)	0.64 (0.05)	0.59 (0.05)	0.61 (0.03)
1-input ablation td ⁷	0.47 (0.1)	0.6 (0.09)	0.51 (0.03)	0.31 (0.12)	0.59 (0.08)	0.39 (0.08)	0.41 (0.1)	0.6 (0.09)	0.47 (0.04)
1-input trained on p1 ⁸	0.72 (0.05)	0.56 (0.05)	0.63 (0.03)	0.57 (0.08)	0.52 (0.07)	0.54 (0.05)	0.66 (0.07)	0.55 (0.05)	0.6 (0.03)
1-input trained on p2 ⁹	0.75 (0.05)	0.5 (0.05)	0.6 (0.02)	0.62 (0.09)	0.45 (0.05)	0.52 (0.03)	0.7 (0.06)	0.49 (0.04)	0.57 (0.02)
1-input regression ¹⁰	0.62 (0.07)	0.64 (0.06)	0.63 (0.03)	0.53 (0.06)	0.55 (0.08)	0.53 (0.04)	0.58 (0.06)	0.62 (0.06)	0.6 (0.03)

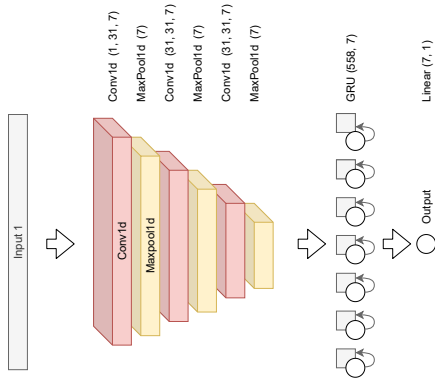


Fig. 9. Final single-input ANN architecture. The dimensions of each layer are provided in parenthesis using the PyTorch nomenclature.

corresponding to the right-hand end of the Pareto front, since it is rather small with only 25.6k parameters. We measure the execution time of this architecture to be 20 ms per forward pass on the Portiloop (vs. 40 ms for the 2-input version).

The selected architecture is described in Figure 9, and its detection performance is summarized in Table I, row (6). Compared to our 2-input model, the single-input model exhibits the same performance, with even a marginal improvement on phase 2, while executing twice as fast. The detailed hyperparameters of this model are provided in Appendix D.

7) *Time-dilation ablation*: We illustrate the importance of using virtual parallelization via time-dilation. This is done by shrinking the time-dilation (set at 168 ms by PMBO) to the minimum, *i.e.*, 20 ms since this is the execution duration of the ANN per forward pass. This removes the virtual parallelization, since the same ANN must now be used for each sample. Therefore, each step of back-propagation reaches 8 times less far back in time during training. The result of this ablation is presented in Table I, row (7). The highly deteriorated results illustrate the importance of time-dilation. This hints at the relevance of looking relatively far back in

time to annotate sleep spindles.

8) *Training and evaluating on different phases*: We now perform an ablation on the MODA dataset itself to highlight a gap between the data of phase 1 (younger subjects) and the data of phase 2 (older subjects). Namely, we train the model on subjects drawn only from phase 1 on the one hand, and on subjects drawn only from phase 2 on the other hand. The results of these experiments are presented in Table I, rows (8, 9). We observe that the ANN trained on phase 1 performs almost as well as the ANN trained on the whole cohort (6) on all subsets, including phase 2, whereas the ANN trained on phase 2 is noticeably worse on all subsets, even including phase 2. We hypothesize that this is because phase 2 has fewer sleep spindle examples, which are furthermore harder to detect. Using phase 2 during training is still useful in terms of generalization. Indeed, the ANN trained on phase 1 only (8) has a slightly worse performance when tested on phase 1 than the ANN trained on the whole cohort (6).

9) *Regression*: All models presented beforehand are classifiers. We also train a regressor with the same architecture, as explained in Section III-F2. There is a subtle difference in what this model measures when compared to our classifiers: whereas classifiers predict whether the signal is a sleep spindle according to the full definition given by MODA (including post-processing), the regressor predicts the mean score given by the experts (excluding post-processing). Since we are primarily interested in classification in this article, we find the threshold that maximizes the f1-score on the binary labels. This experiment is presented in Appendix E. We find that the optimal threshold is 0.27 for phase 1, 0.23 for phase 2 and 0.26 for the whole cohort. We then evaluate the regressor with these thresholds on the classification task and report the results in Table I, row (10). These results are slightly weaker than those of the classifier (6). We surmise that this effect comes from the post-processing steps performed by MODA to compute the binary labels. We choose the 1-input classifier (6) for the remainder of this article.

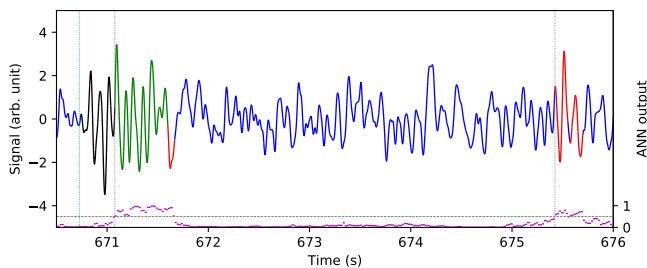


Fig. 10. Stimulation with a 0.5 threshold. The color code is the same as Figure 2, with false positives being additionally displayed in red. Note the first part of the spindle is not detected (false negative), which introduces an ANN software delay. In addition, a small portion of the signal after the spindle is still detected as such (false positive), but it has no impact on our stimulation procedure. Finally, another portion of the signal that was not annotated as a spindle by MODA is detected as a spindle by our model (false positive), generating an undesirable stimulus is generated.

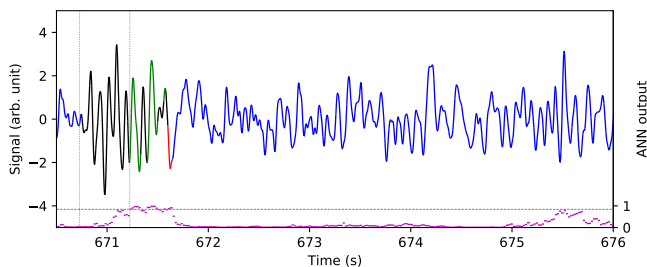


Fig. 11. Stimulation with a 0.84 threshold.

B. Real-time stimulation

The performance measured in Section IV-A is not entirely representative of the performance on the final task. So far, we have only measured the capability of the model to annotate each data point of the signal individually. Yet, we want the ability to send one single stimulation per sleep spindle.

1) *Qualitative results:* Figure 10 shows an example of imperfect sleep spindle detection and stimulation using our ANN (see Appendix B for more details on failure modes).

Although we chose using a classifier as opposed to a regressor, it is still possible to reduce incorrect stimulation by fine-tuning the detection threshold (0.5 by default). Figure 11 shows an increased threshold reduces the incorrect stimulation. However, a high threshold worsens the detection delay since it increases the number of false negatives at spindle onset.

2) *Quantitative results:* Although the results presented in Section IV-B1 focus on the ANN detection delay, we must take in consideration the other sources of delay, *i.e.*, the software delay from FIRs (40 ms), the ANN forward pass duration (20 ms) and the stimulation hardware delay, to measure our real stimulation performance. The auditory stimulation delay in the Portiloop is 4 ms, for a total constant delay of 64 ms.

From now on, we redefine: (a) True positive: the first stimulus sent within the duration of a spindle, taking this additional delay into account; (b) False positive: any other stimulus; (c) False negative: any spindle that does not receive a stimulus within its labeled duration.

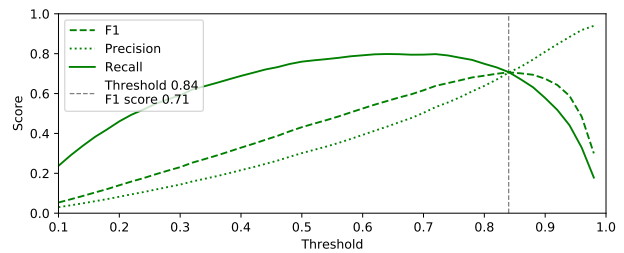


Fig. 12. Evolution of the actual stimulation performance w.r.t. the chosen detection threshold.

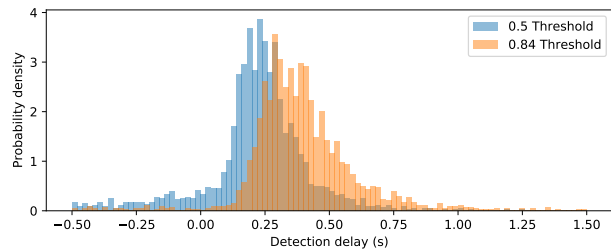


Fig. 13. Distribution of stimulation delays for a classifier with 0.5 and 0.84 threshold. Delays are negative when spindles are stimulated in advance.

Figure 12 displays the detection performance (taking all delays into account) of our final device. We compute the stimulation precision, recall and f1-score according to the aforementioned definitions of true positives, false positives and false negatives. This provides a visualization of possible trade-offs in terms of how many spindles we want to stimulate (recall) versus how sure we want to be that all stimuli are relevant (precision). In terms of f1-score, the best such trade-off is attained at a threshold of 0.84 with our model, giving a precision and a recall of 0.71.

We further study the timing performance of our system. Figure 13 displays the distribution of stimulation delays, *i.e.*, the distribution of the stimulus being closest to the beginning of each sleep spindle, all delays being taken into account. Some of these delays are negative, as spindles are sometimes stimulated in advance (NB: we count these as false positives, which slightly harms our reported results). Moreover it shows the effect of increasing the detection threshold of our model on the stimulation delays. According to Figure 12, choosing a 0.84 detection threshold over the 0.5 default classification threshold in our ANN yields a better stimulation f1-score and in particular much more precise stimuli, but this comes at the price of slightly shifting the stimulation delay distribution to the right, *i.e.*, introducing some additional delay to the stimulation, as previously seen in Figure 11.

Finally, we estimate the Portiloop energy efficiency by running our final sleep spindle stimulation device continuously, powered by a fully-charged 20000 mAh battery. The battery dies out after 26 hours and 22 minutes, suggesting that our power consumption is roughly 756 mA.

V. DISCUSSION AND FUTURE WORK

The Portiloop system can be adapted to any application of EEG closed-loop stimulation. Although classifiers are most relevant in our case study, it would be straightforward to

extend the Portiloop to quantitative tasks using regressors instead, as seen in Section IV-A9.

As opposed to classical heuristics, our deep learning-based approach does not require specific knowledge of the phenomenon of interest when defining the classifier, nor requires a way to extract the relevant information. Instead, a large dataset of annotated signal suffices to derive a high-performance model that detects complex patterns such as sleep spindles. Once trained, techniques such as Integrated Gradients [50] can be used to better understand and fine-tune the ANN. Moreover, these techniques may help experts by revealing unknown dependencies in neural activity, as we hint in Appendix A.

We have introduced PMBO to derive Pareto-optimal architectures in a parallel fashion. Although the algorithm produces high-performance lightweight architectures, we note that the predictions of the meta-learner are often near-constant in well-performing areas of the search space, suggesting that the meta-model could not further predict the software cost. We surmise that this is due to the large variance in model performance from one training session to another. This might be alleviated by training the same model several times, but we forbade this in our implementation to speed up the search.

Although we compare our architecture to the SpindleNet architecture, we did not have access to their weights and thus we could not compare their original model with ours on the MODA dataset. Instead, we retrained their architecture from scratch on MODA, using our own pipeline. Contrary to Kulkarni *et al.* [29], we could remove the envelope and power inputs without harming the performance of our models. During the course of our work, we have noticed that our 1-input model was less robust to shrinking the time-dilation than our 2-input model. Since the baseline does not use time-dilation, it cannot reach far back in time. We believe that this is important for the model to retrieve the information contained in these additional inputs. Note that it is necessary not to reduce the capacity of the model (*e.g.*, by cutting a branch of the ANN instead of duplicating inputs) when performing the ablation study, which Kulkarni *et al.* might have overlooked.

While the MODA dataset provides high-quality labels, training on a bigger dataset of similar quality would likely further improve the performance of our models. Expanding MODA is a relevant avenue for future work, as is implementing sim-to-real transfer, because the EEG acquisition and signal may differ somewhat from the training data. Transfer can be achieved with techniques such as domain randomization [51]. Alternatively, a dataset can be collected on the target device and annotated following the same protocol as MODA.

Long term, we intend to target specific regions of sleep spindles for stimulation. This harder task will likely involve labeling these regions and developing more advanced RNNs/Transformers so as to consistently predict sleep spindles before they even start. Although our model does use information far back in time to make predictions (see Appendix A), we believe that the main role currently played by the RNN is to accumulate information regarding whether the last few windows were spindles or not, rather than actually predicting the future (see Appendix B). Such models will likely be more complex and computationally hungry. We will integrate a TPU

in the system, as part of an ad-hoc PCB that will replace the prototyping board currently used, further miniaturizing the Portiloop. In general, finding an optimal model for a given Portiloop application involves either retraining our ANN, or re-executing PMBO with a new architecture. Both activities can be done by interested practitioners.

VI. CONCLUSION

In this article, we introduce the Portiloop, a device that enables the real-time detection and stimulation of patterns of interest in EEG signal. Our system is open-source, portable, low-cost, and can be tailored for many such applications. The Portiloop enables implementing task-specific deep learning-based detectors directly in efficient hardware circuitry. This is made possible via an FPGA and a C++ HLS library that we open-source along with the rest of our code. We propose a pipeline to design neural architectures that are relevant for processing EEG signal in real time. We further propose PMBO, an algorithm that automates the process of finding efficient such models, using one to many parallel workers. We demonstrate our proposed system on the closed-loop stimulation of sleep spindles, a difficult task of high relevance for the neuroscience community. Our resulting system is the first portable device to be able to detect and stimulate sleep spindles in real time with a f1-score of 0.71, measured on MODA, a dataset renowned for the reliability of its labels. In the long range, the Portiloop will help the neuroscience community non-invasively explore brain functions, such as the role of sleep spindles in memory consolidation.

ACKNOWLEDGMENT

We thank Karine Lacourse for expert advice on spindle detection, and the MODA team for database access. Figures 1 and 3 use icons from <https://flaticon.com>.

REFERENCES

- [1] H.-V. V. Ngo, T. Martinetz, J. Born, and M. Mölle, "Auditory Closed-Loop Stimulation of the Sleep Slow Oscillation Enhances Memory," *Neuron*, vol. 78, no. 3, pp. 545–553, May 2013.
- [2] U. Ha and H.-J. Yoo, "A multimodal drowsiness monitoring ear-module system with closed-loop real-time alarm," in *2016 IEEE Biomedical Circuits and Systems Conference (BioCAS)*, Oct. 2016, pp. 536–539.
- [3] A. von Lüthmann, J. Addesa, S. Chandra, A. Das, M. Hayashibe, and A. Dutta, "Neural interfacing non-invasive brain stimulation with NIRS-EEG joint imaging for closed-loop control of neuroenergetics in ischemic stroke," in *2017 8th International IEEE/EMBS Conference on Neural Engineering (NER)*, May 2017, pp. 349–353.
- [4] N. Kosmyna and P. Maes, "Attentivu: An EEG-based closed-loop biofeedback system for real-time monitoring and improvement of engagement for personalized learning," *Sensors*, vol. 19, no. 23, 2019.
- [5] G. Zarubin, C. Gundlach, V. Nikulin, and M. Bogdan, "Real-time phase detection for EEG-based tACS closed-loop system," in *6th International Congress on Neurotechnology, Electronics and Informatics*, Seville, Spain, 2018, pp. 13–20.
- [6] S. Shirinpour, I. Alekseichuk, K. Mantell, and A. Opitz, "Experimental evaluation of methods for real-time EEG phase-specific transcranial magnetic stimulation," *J. Neural Engineering*, vol. 17, no. 4, 2020.
- [7] C. Zrenner, P. Belardinelli, F. Müller-Dahlhaus, and U. Ziemann, "Closed-loop neuroscience and non-invasive brain stimulation: a tale of two loops," *Frontiers in cellular neuroscience*, vol. 10, p. 92, 2016.
- [8] A. Vassileva, D. van Blooijis, F. Leijten, and G. Huiskamp, "Neocortical electrical stimulation for epilepsy: Closed-loop versus open-loop," *Epilepsy research*, vol. 141, pp. 95–101, 2018.

- [9] J. Choi, M. Kwon, and S. C. Jun, "A systematic review of closed-loop feedback techniques in sleep studies—related issues and future directions," *Sensors*, vol. 20, no. 10, p. 2770, 2020.
- [10] K. D. Fehér, M. Wunderlin, J. G. Maier, E. Hertenstein, C. Schneider, C. Mikutta, M. A. Züst, S. Klöppel, and C. Nissen, "Shaping the slow waves of sleep: A systematic and integrative review of sleep slow wave modulation in humans using non-invasive brain stimulation," *Sleep medicine reviews*, p. 101438, 2021.
- [11] F. Salfi, A. D'Atri, D. Tempesta, L. De Gennaro, and M. Ferrara, "Boosting slow oscillations during sleep to improve memory function in elderly people: A review of the literature," *Brain Sciences*, vol. 10, no. 5, p. 300, 2020.
- [12] M. O. Harrington and S. A. Cairney, "Sounding it out: auditory stimulation and overnight memory processing," *Current Sleep Medicine Reports*, 2021.
- [13] T. O. Bergmann and B. P. Staresina, "Neuronal oscillations and reactivation subserving memory consolidation," in *Cognitive neuroscience of memory consolidation*. Springer, 2017, pp. 185–207.
- [14] B. Rasch and J. Born, "About sleep's role in memory," *Physiological reviews*, 2013.
- [15] S. M. Fogel and C. T. Smith, "Learning-dependent changes in sleep spindles and stage 2 sleep," *Journal of sleep research*, vol. 15, no. 3, pp. 250–255, 2006.
- [16] M. Lafortune, J.-F. Gagnon, N. Martin, V. Latreille, J. Dubé, M. Bouchard, C. Bastien, and J. Carrier, "Sleep spindles and rapid eye movement sleep as predictors of next morning cognitive performance in healthy middle-aged and older participants," *Journal of sleep research*, vol. 23, no. 2, pp. 159–167, 2014.
- [17] S. Fogel, C. Vien, A. Karni, H. Benali, J. Carrier, and J. Doyon, "Sleep spindles: a physiological marker of age-related changes in gray matter in brain regions supporting motor skill memory consolidation," *Neurobiology of aging*, vol. 49, pp. 154–164, 2017.
- [18] L. M. J. Fernandez and A. Lüthi, "Sleep Spindles: Mechanisms and Functions," *Physiological Reviews*, vol. 100, no. 2, pp. 805–868, 2020.
- [19] K. R. Peters, L. B. Ray, S. Fogel, V. Smith, and C. T. Smith, "Age differences in the variability and distribution of sleep spindle and rapid eye movement densities," *PLoS one*, vol. 9, no. 3, p. e91047, 2014.
- [20] S. Purcell, D. Manoach, C. Demanuele, B. Cade, S. Mariani, R. Cox, G. Panagiotaropoulou, R. Saxena, J. Pan, J. Smoller *et al.*, "Characterizing sleep spindles in 11,630 individuals from the national sleep research resource," *Nature communications*, vol. 8, no. 1, pp. 1–16, 2017.
- [21] K. Lacourse, J. Delfrate, J. Beaudry, P. Peppard, and S. C. Warby, "A sleep spindle detection algorithm that emulates human expert spindle scoring," *J. Neuroscience Methods*, vol. 316, pp. 3–11, Mar. 2019.
- [22] K. Lacourse, B. Yetton, S. Mednick, and S. C. Warby, "Massive online data annotation, crowdsourcing to generate high quality sleep spindle annotations from EEG data," *Sci Data*, vol. 7, no. 1, p. 190, Jun. 2020.
- [23] P. Albouy, A. Weiss, S. Baillet, and R. J. Zatorre, "Selective entrainment of theta oscillations in the dorsal stream causally enhances auditory working memory performance," *Neuron*, vol. 94, no. 1, pp. 193–206, 2017.
- [24] C. M. McCrimmon, J. L. Fu, M. Wang, L. S. Lopes, P. T. Wang, A. Karimi-Bidhendi, C. Y. Liu, P. Heydari, N. Nenadic, and A. H. Do, "Performance Assessment of a Custom, Portable, and Low-Cost Brain-Computer Interface Platform," *IEEE Transactions on Biomedical Engineering*, vol. 64, no. 10, pp. 2313–2320, 2017.
- [25] S. Zotou, G. K. Kostopoulos, and T. A. Antonakopoulos, "Real-time Spindles Detection for Acoustic Neurofeedback," in *Brain Function Assessment in Learning*, ser. Lecture Notes in Computer Science, C. Frasson and G. Kostopoulos, Eds. Cham: Springer International Publishing, 2017, pp. 159–168.
- [26] H.-V. V. Ngo, M. Seibold, D. C. Boche, M. Mölle, and J. Born, "Insights on auditory closed-loop stimulation targeting sleep spindles in slow oscillation up-states," *Journal of Neuroscience Methods*, vol. 316, pp. 117–124, Mar. 2019.
- [27] L. L. Chen, R. Madhavan, B. I. Rapoport, and W. S. Anderson, "Real-time brain oscillation detection and phase-locked stimulation using autoregressive spectral estimation and time-series forward prediction," *IEEE Trans. on Biomed. Eng.*, vol. 60, no. 3, pp. 753–762, 2013.
- [28] R. Xu, N. Jiang, C. Lin, N. Mrachacz-Kersting, K. Dremstrup, and D. Farina, "Enhanced low-latency detection of motor intention from EEG for closed-loop brain-computer interface applications," *IEEE Transactions on Biomedical Engineering*, vol. 61, no. 2, pp. 288–296, 2014.
- [29] P. M. Kulkarni, Z. Xiao, E. J. Robinson, A. S. Jami, J. Zhang, H. Zhou, S. E. Henin, A. A. Liu, R. S. Osorio, J. Wang, and Z. Chen, "A deep learning approach for real-time detection of sleep spindles," *J. Neural Eng.*, vol. 16, no. 3, p. 036004, Jun. 2019.
- [30] N. I. Tapia and P. A. Estévez, "RED: Deep Recurrent Neural Networks for Sleep EEG Event Detection," *arXiv:2005.07795*, May 2020.
- [31] C. O'Reilly, N. Gosselin, J. Carrier, and T. Nielsen, "Montreal Archive of Sleep Studies: An open-access resource for instrument benchmarking and exploratory research," *Journal of Sleep Research*, vol. 23, no. 6, pp. 628–635, 2014.
- [32] F. Ferrarelli, R. Huber, M. J. Peterson, M. Massimini, M. Murphy, B. A. Riedner, A. Watson, P. Bria, and G. Tononi, "Reduced Sleep Spindle Activity in Schizophrenia Patients," *AJP*, vol. 164, no. 3, pp. 483–492, Mar. 2007.
- [33] M. Mölle, L. Marshall, S. Gais, and J. Born, "Grouping of Spindle Activity during Slow Oscillations in Human Non-Rapid Eye Movement Sleep," *J. Neurosci.*, vol. 22, no. 24, pp. 10941–10947, Dec. 2002.
- [34] N. Martin, M. Lafortune, J. Godbout, M. Barakat, R. Robillard, G. Poirier, C. Bastien, and J. Carrier, "Topography of age-related changes in sleep spindles," *Neurobiology of Aging*, vol. 34, no. 2, pp. 468–476, Feb. 2013.
- [35] E. J. Wamsley, M. A. Tucker, A. K. Shinn, K. E. Ono, S. K. McKinley, A. V. Ely, D. C. Goff, R. Stickgold, and D. S. Manoach, "Reduced Sleep Spindles and Spindle Coherence in Schizophrenia: Mechanisms of Impaired Memory Consolidation?" *Biological Psychiatry*, vol. 71, no. 2, pp. 154–161, Jan. 2012.
- [36] L. Ray, S. Sockeel, M. Soon, A. Bore, A. Myhr, B. Stojanoski, R. Cusack, A. M. Owen, J. Doyon, and S. Fogel, "Expert and crowd-sourced validation of an individualized sleep spindle detection method employing complex demodulation and individualized normalization," *Front. Hum. Neurosci.*, vol. 9, 2015.
- [37] A. Parekh, I. W. Selesnick, D. M. Rapoport, and I. Ayappa, "Detection of K-complexes and sleep spindles (DETOKS) using sparse optimization," *Journal of Neuroscience Methods*, vol. 251, pp. 37–46, Aug. 2015.
- [38] N. Yasuhara, T. Natori, M. Hayashi, and N. Aikawa, "A Study on Automatic Detection of Sleep Spindles using a Long Short-Term Memory Network," in *2019 IEEE 62nd International Midwest Symposium on Circuits and Systems (MWSCAS)*, Aug. 2019, pp. 45–48.
- [39] D. Tan, R. Zhao, J. Sun, and W. Qin, "Sleep spindle detection using deep learning: A validation study based on crowdsourcing," in *37th IEEE Engineering in Medicine and Biology Conference (EMBC)*, Aug. 2015, pp. 2828–2831.
- [40] *Pyng Z2 Reference Manual*, TUL, 2019, rev. 1.1.
- [41] *ADSI299-x Low-Noise, 4-, 6-, 8-Channel, 24-Bit, Analog-to-Digital Converter for EEG and Biopotential Measurements datasheet*, Texas Instrument, 2012, rev. C (2017).
- [42] M. Vohra and S. Fasciani, "PYNQ-Torch: A framework to develop PyTorch accelerators on the PYNQ platform," in *IEEE International Symposium on Signal Processing and Information Technology (ISSPIT)*, Dec. 2019, pp. 1–6.
- [43] J. Chung, C. Gulcehre, K. Cho, and Y. Bengio, "Empirical Evaluation of Gated Recurrent Neural Networks on Sequence Modeling," *arXiv:1412.3555 [cs]*, Dec. 2014.
- [44] S. Yang, X. Yu, and Y. Zhou, "LSTM and GRU Neural Network Performance Comparison Study: Taking Yelp Review Dataset as an Example," in *2020 International Workshop on Electronic Communication and Artificial Intelligence (IWECAI)*, Jun. 2020, pp. 98–101.
- [45] A. Vaswani, N. Shazeer, N. Parmar, J. Uszkoreit, L. Jones, A. N. Gomez, Ł. Kaiser, and I. Polosukhin, "Attention is all you need," in *Advances in neural information processing systems*, 2017, pp. 5998–6008.
- [46] Z. Yin, W. Gross, and B. H. Meyer, "Probabilistic sequential multi-objective optimization of convolutional neural networks," in *2020 Design, Automation & Test in Europe Conference & Exhibition (DATE)*. IEEE, 2020, pp. 1055–1060.
- [47] S. Chang, Y. Zhang, W. Han, M. Yu, X. Guo, W. Tan, X. Cui, M. Witbrock, M. Hasegawa-Johnson, and T. S. Huang, "Dilated recurrent neural networks," *arXiv preprint arXiv:1710.02224*, 2017.
- [48] Y. Yang, K. Zha, Y.-C. Chen, H. Wang, and D. Katabi, "Delving into deep imbalanced regression," *arXiv preprint arXiv:2102.09554*, 2021.
- [49] C. Iber, S. Ancoli-Israel, A. L. Chesson, S. F. Quan *et al.*, *The AASM manual for the scoring of sleep and associated events: rules, terminology and technical specifications*. American academy of sleep medicine Westchester, IL, 2007, vol. 1.
- [50] M. Sundararajan, A. Taly, and Q. Yan, "Axiomatic attribution for deep networks," in *International Conference on Machine Learning*. PMLR, 2017, pp. 3319–3328.
- [51] J. Tobin, R. Fong, A. Ray, J. Schneider, W. Zaremba, and P. Abbeel, "Domain randomization for transferring deep neural networks from simulation to the real world," in *International conference on intelligent robots and systems (IROS)*. IEEE, 2017, pp. 23–30.

APPENDIX A
MODEL-BASED EXPLANATION OF SLEEP SPINDLES

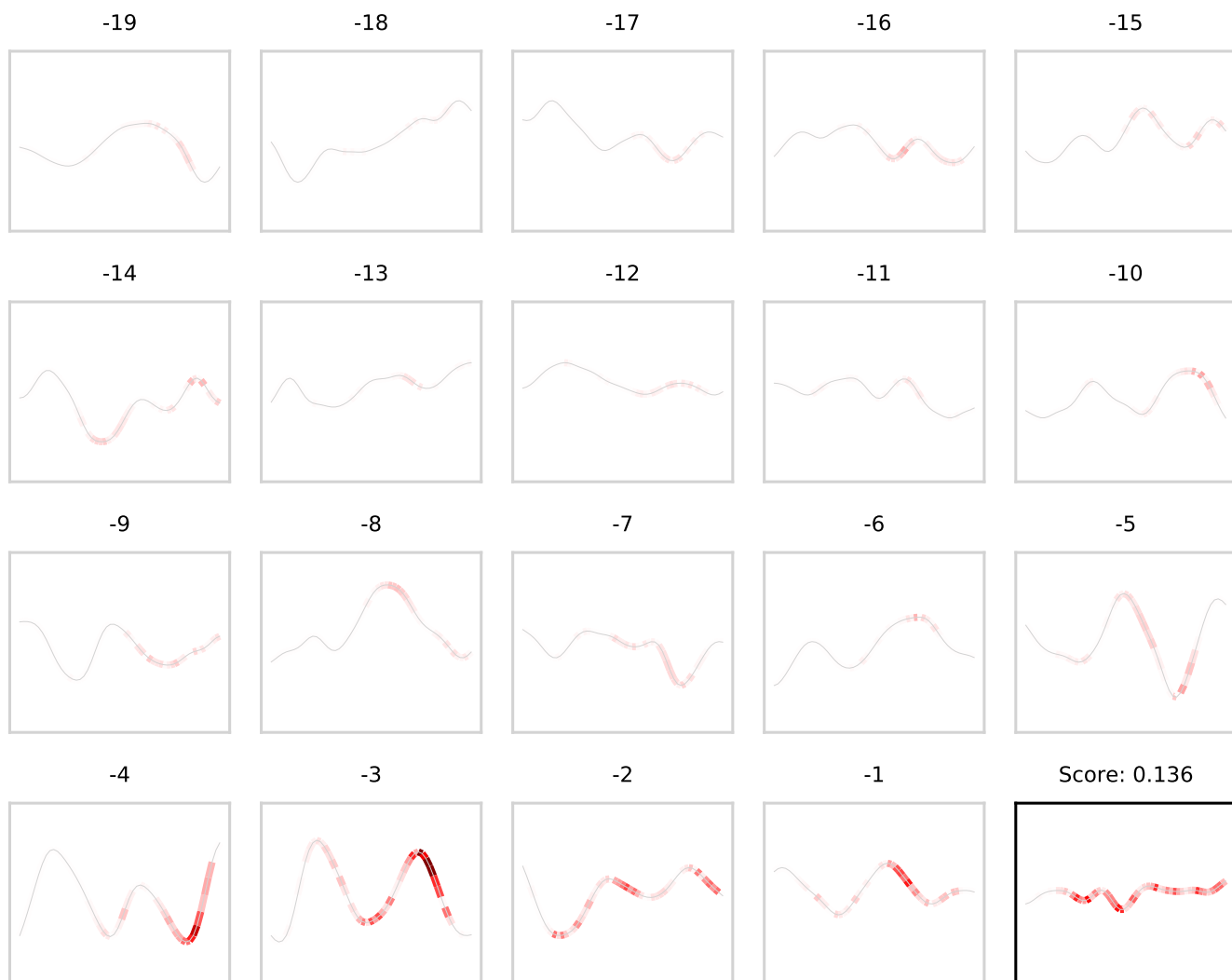


Fig. 14. Integrated gradients (classifier ANN output: 0.136). The *integrated gradients* algorithm enables exploring why the model takes a given decision (the more a portion of the signal is represented in red, the highest its influence on the current output of the ANN). Grey windows are past inputs, whereas the black window is the current input: the past influences the current output due to the RNN. Here, the model finds that it is looking at the aftermath of a sleep spindle. With our time dilation and window size, a small portion of the window overlaps from one sample to the next. We see that this portion (at the left-hand side of each window) is in fact ignored by the model. Therefore, it is probably possible to shrink our model even more, although PMBO did not find this. In the future, this type of visualizations might also help experts better understand what sleep spindles are by revealing unknown influences.

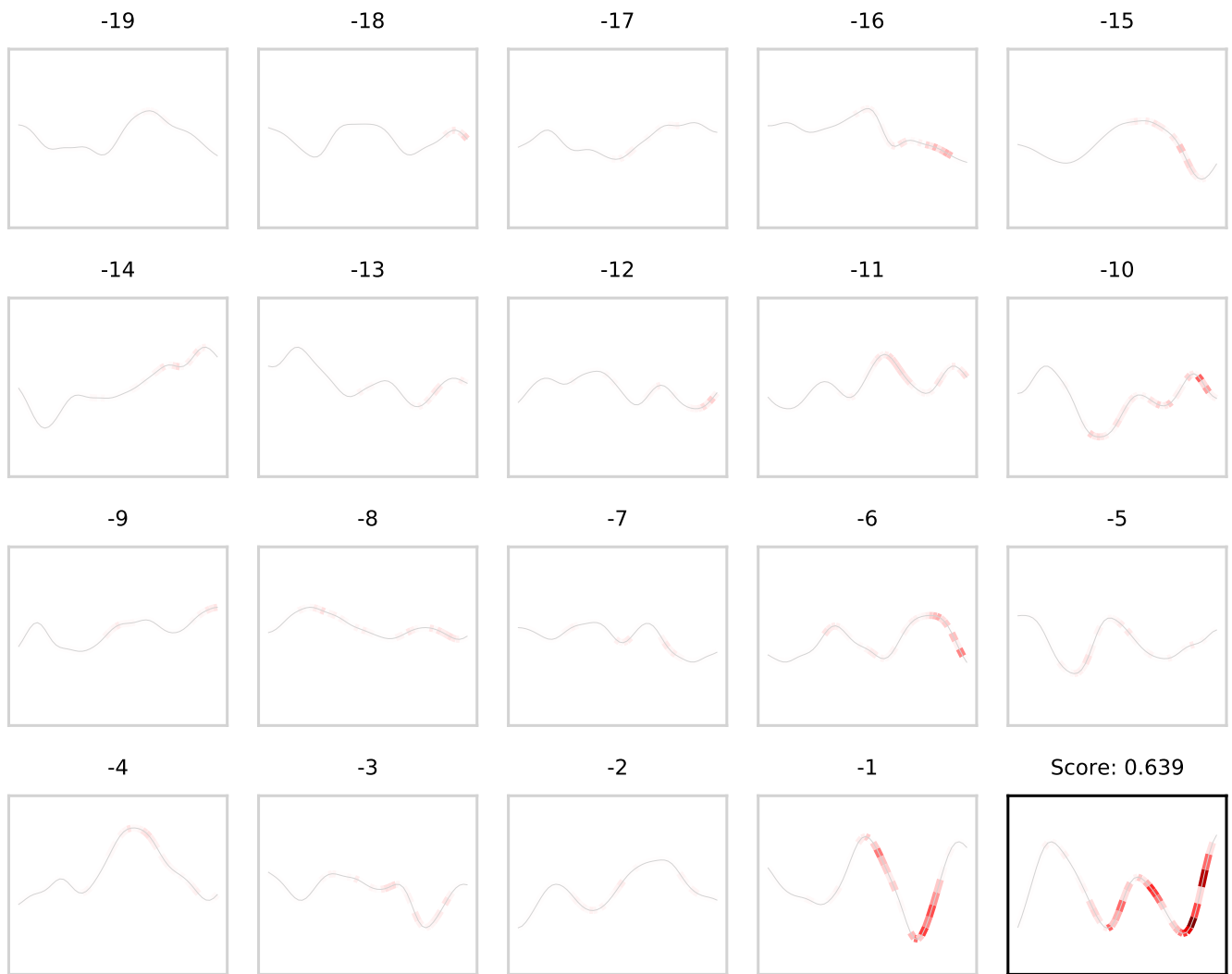


Fig. 15. Integrated gradients (classifier ANN output: 0.639). The current window is within an actual sleep spindle. The model mainly focuses on the spindle itself, but also a few events that happened further back in time, to make its decision.

APPENDIX B
STIMULATION VISUALIZATIONS

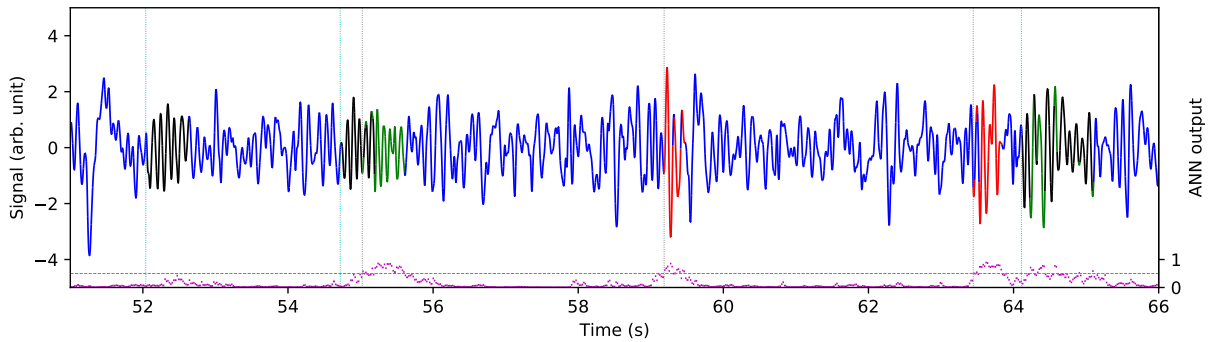


Fig. 16. Different stimulation failure modes (classifier with threshold 0.5). Blue: no sleep spindle and no detection. Black: sleep spindle not detected. Green: sleep spindle correctly detected. Red: detection where the signal is not a spindle. Vertical blue: beginning of a spindle. Vertical grey: stimulation. Magenta: ANN output. Horizontal grey: detection threshold. This figure illustrates typical ‘failure’ cases of our final sleep spindle stimulating device. False negative: the first spindle is missed because the threshold is too big. True positive: the second spindle is correctly stimulated. False positive: a part of the signal not labeled as a sleep spindle by MODA is detected as a spindle by the device and stimulated. Almost true positive: the sleep spindle is stimulated in advance (NB: we count this case as a false positive).

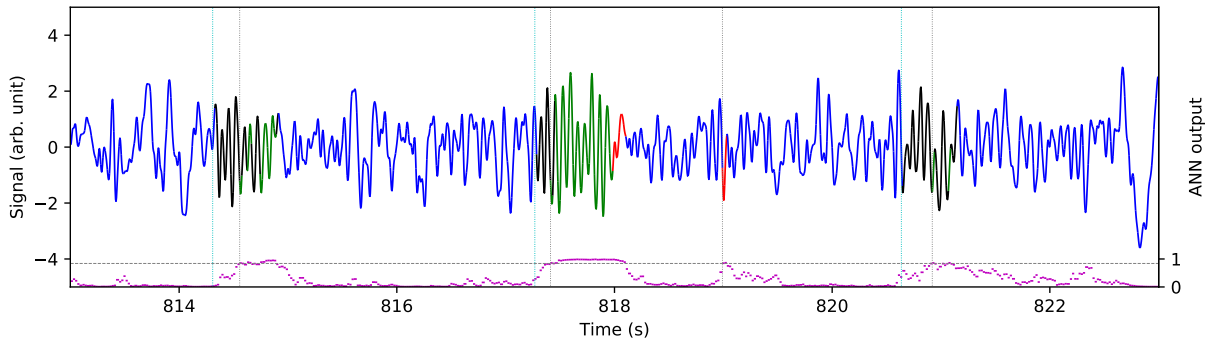


Fig. 17. Classifier with threshold 0.84, success example. Same color code as Figure 16. Increasing the detection threshold from 0.5 to 0.84 removes most false positive stimuli (vertical grey not following vertical blue).

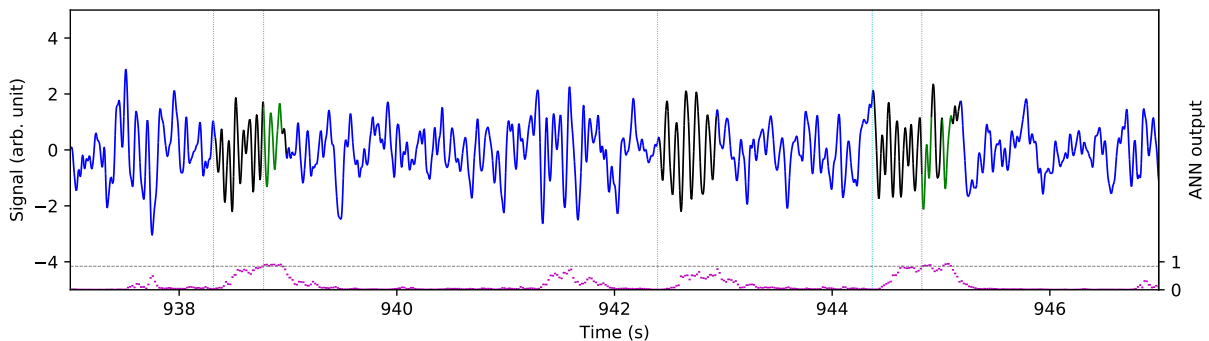


Fig. 18. Classifier with threshold 0.84, failure example. Same color code as Figure 16. Increasing the detection threshold comes with more false negative stimuli (vertical blue not followed by vertical grey).

APPENDIX C PMBO HYPERPARAMETERS

Table II. Hyperparameters used for PMBO

hyperparameter	selected value
range cost hardware	1000-80000
noise type 1	0,25
noise type 2	0,1
m	200
meta network type	MLP
# layers meta network	3
hidden size meta network	200
optimizer meta network	SGD
learning rate meta network	0.05
weight decay meta network	0.01

Two types of noise are used in our implementation of PMBO to foster exploration of the hyperparameter space:

- noise type 1: portion of the m sampled models that are sampled randomly in the whole hyperparameter space, instead of in a Gaussian around the last completed experiment.
- noise type 2: portion of the time when a model is sampled randomly in the m models, instead of being selected by its Pareto efficiency.

The ANN used for our meta model is a simple Multi-Layer Perceptron (MLP) of 3 fully connected layers. The hyperparameters we use in PMBO are summarized in Table II.

APPENDIX D MODEL HYPERPARAMETERS

Table III. Hyperparameters used to train the final model

Hyperparameter	Selected value	PMBO
Training		
optimizer	AdamW	
# epochs max	150	
epochs before early stopping	20	
early stopping running average factor	0,1	
batches per epoch	1000	
batch size	256	X
dropout on first layer	False	
dropout factor	0,5	
adam learning rate	0,0005	X
adam weight decay	0,01	
balancing mode	oversampling	
type of training	classification	
sequence length	50	
Architecture		
window size (s)	0,216	X
time dilation (s)	0,168	X
# CNN layers	3	X
# CNN channels	31	X
stride convolution	1	X
kernel size convolution	7	X
dilation convolution	1	X
stride max pooling	1	X
kernel size max pooling	1	X
dilation max pooling	1	X
RNN layers	1	X
RNN hidden size	7	X

The hyperparameters we use in our final model are listed in Table III. Hyperparameters that were chosen by PMBO are marked with a cross under the PMBO column.

APPENDIX E
BEST THRESHOLD FOR CLASSIFIERS AND REGRESSORS

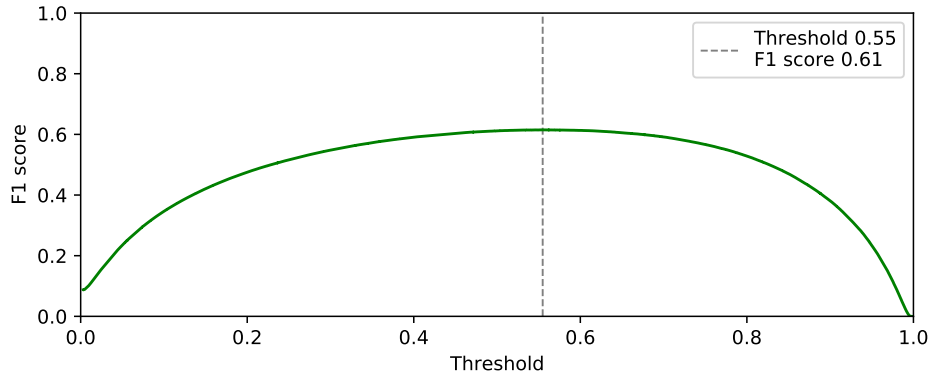


Fig. 19. F1 score evolution with threshold variation on classification

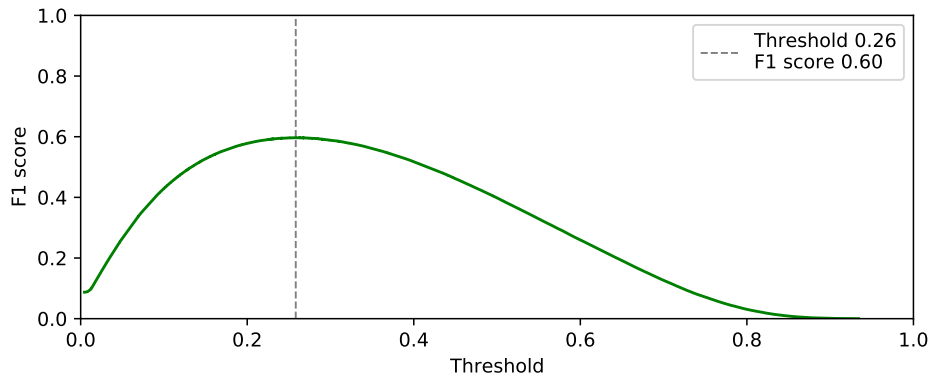


Fig. 20. F1 score evolution with threshold variation on regression

APPENDIX F
DETECTION DELAY DISTRIBUTIONS

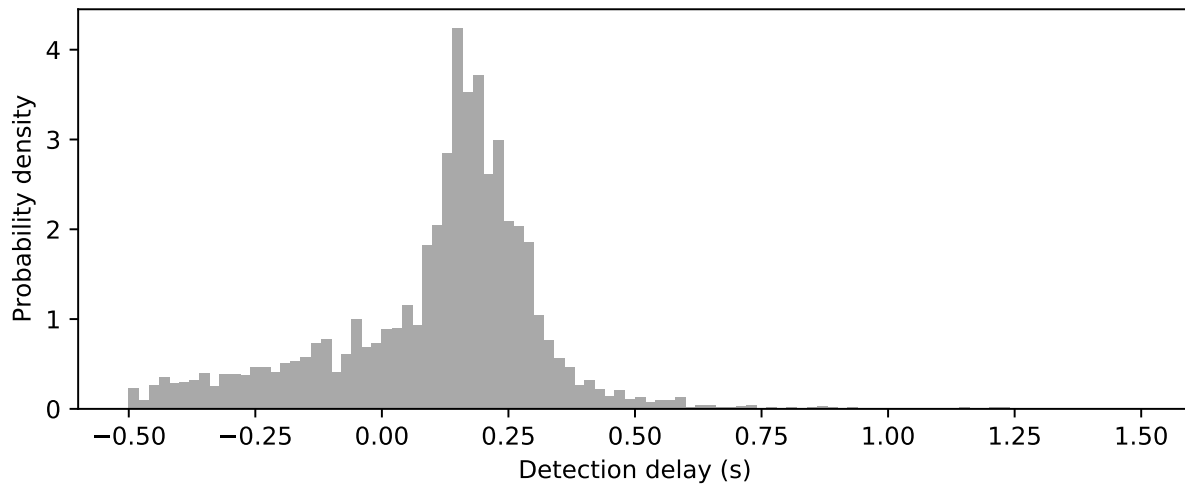


Fig. 21. Stimulation histogram for 1 input network classification with a 0.25 threshold

APPENDIX G

2-INPUT NETWORK ARCHITECTURE

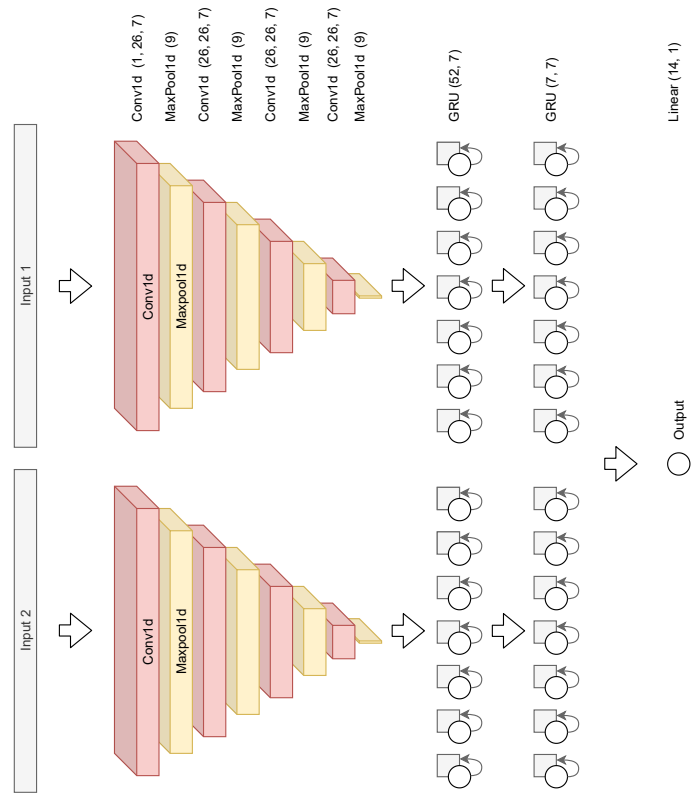


Fig. 22. 2-input neural network architecture. This architecture consists of two sequences of CNN and RNN. The first sequence processes the cleaned raw signal (input 1), whereas the second processes the envelope (input 2). The latent features from both branches are concatenated and fed to a fully connected layer to yield the output of the ANN.